Optical band gap hierarchy in a magnetic oxide: Electronic structure of $NiFe_2O_4$

Q. - C. Sun,[1] H. Sims,[2] D. Mazumdar,[1,2] J. X. Ma,[2] B. S. Holinsworth,[1] K. R. O'Neal,[1] G. Kim,[2,*] W. H. Butler,[2] A. Gupta,[2] and J. L. Musfeldt[1]

[1]*Department of Chemistry, University of Tennessee, Knoxville, Tennessee 37996, USA*

[2]*Center for Materials for Information Technology, University of Alabama, Tuscaloosa, Alabama 35487, USA*

(Received 5 April 2012; revised manuscript received 5 September 2012; published 5 November 2012)

We combined first-principles calculations with optical spectroscopy and variable-temperature film growth techniques to comprehensively investigate the electronic structure of $NiFe_2O_4$. We find this system to be an indirect-gap material in the minority channel, with two higher-energy direct-gap structures in the minority and majority channels, respectively. An analysis of states near the band edge simultaneously exposes both the charge transfer and Mott limits of the Zaanen-Sawatzky-Allen classification scheme. The gap hierarchy is well suited for spintronics applications.

DOI: 10.1103/PhysRevB.86.205106 PACS number(s): 75.76.+j, 71.15.Mb, 75.50.Gg, 78.20.−e

I. INTRODUCTION

One of the many attractive features of complex oxides is their unique and tunable functionalities. Magnetic insulators are garnering particular interest in this regard.[1] Apart from their traditional usage in microwave devices, many newer paradigms are emerging, especially in the area of spintronics, where magnetic insulators can play a central role in generating highly spin-polarized currents.[2–4] It has also been proposed that the split-band nature of ferromagnetic insulators can help realize an ON/OFF ratio large enough for logic operations.[5,6] Moreover, by virtue of their insulating nature, spin-bearing thermal magnons have been predicted to improve spin-transfer torque device efficiencies.[7] Eventual realization of these ideas is inherently linked with a quantitative understanding of bulk and interfacial electronic properties. Due to their high Curie temperatures, spinel ferrites like $NiFe_2O_4$ are attractive candidate systems.[8,9] Understanding the role of electron correlation in these and other oxides is, however, a major challenge.[10–18] Previous work demonstrated that an on-site Hubbard U parameter is needed to correctly describe the insulating ground state of $NiFe_2O_4$ within the local-density approximation (LDA) of density functional theory (DFT).[19] Magnetostructural and cation inversion effects have also attracted attention.[20,22] Moreover, there is no consistent experimental data on the optical band gap of $NiFe_2O_4$ with values as low as 0.33 eV and as high as 3.7 eV reported in the literature.[23–27] These discrepancies make elusive a consistent view of the electronic structure.

In this work, we synergistically combine first-principles calculations with optical spectroscopies and epitaxial thin-film growth techniques to resolve this controversy. To treat electron-correlation effects, we reached beyond LDA techniques by adopting LDA + U and hybrid functional approaches,[13,14] the consistency of which reveals the microscopic nature of the observed optical excitations. Our measurements show $NiFe_2O_4$ to be an indirect band gap system ($2\Delta_{indir}$ = 1.6 eV), which theory assigns to the minority (spin-down) channel. The optical response also displays two different direct gaps belonging to the minority and majority channels, respectively. Taken together, our work reveals states near the band edge that display both charge transfer and Mott character, a hierarchy of charge gaps that overlaps well with the solar spectrum, and a framework for understanding the electronic structure of spinel ferrites that advances the use of these materials in spintronics applications.

II. METHODS

Electronic band structure calculations were performed with the VIENNA AB INITIO SIMULATION PACKAGE (VASP)[28,29] on a relaxed 14-atom primitive $NiFe_2O_4$ cell using LDA + U and hybrid functionals [Heyd-Scuseria-Ernzerhof (HSE06)].[13,14,30] We performed calculations within both local spin-density approximation (LSDA) + U (applying the fully local double-counting term and using U_{eff} = 4.5 eV for Fe and 4.0 eV for Ni, which agree with the values used in Ref. 19 and are close to those obtained from constrained LDA)[31] and the HSE06[13,14,30] screened hybrid exchange functional approximation to the DFT. We use the projector augmented wave (PAW)[32] pseudopotentials from Kresse and Joubert.[28,29] In all cases, we employed a plane-wave cutoff of 400 eV. We use a Γ-centered 8 × 8 × 8 k-mesh in all calculations, with a coarser 4 × 4 × 4 k-mesh for the computation of the Hartree-Fock exchange energy.

A series of epitaxial $NiFe_2O_4$ thin films with thicknesses between 150 and 270 nm were prepared on (001)-orientated $MgAl_2O_4$ substrates at growth temperatures of 690, 550, 400, and 250 °C using the pulsed laser deposition technique. Oxygen pressure during growth was kept at 10 mTorr mixed with 5%–10% of ozone and a laser fluence of 2 J/cm^2. The base pressure of the deposition chamber was 2×10^{-7} Torr. A detailed characterization of these samples has been reported in earlier work.[33]

The 300 K transmittance and reflectance measurements on $NiFe_2O_4$ thin films[33] prepared at different temperatures as well as the independent substrate were carried out using a Perkin-Elmer Lambda-900 spectrometer (3000–190 nm; 0.41–6.53 eV). The optical properties were determined by combining Glover-Tinkham and Kramers-Kronig techniques.[34,35] The gap analysis and color rendering calculation employed the absorption,[36,37] whereas the imaginary part of the dielectric function was compared with our calculations.

III. RESULTS AND DISCUSSION

Figures 1(a) and 1(b) display the density of states as obtained with LSDA + U and HSE06. There is good qualitative agreement between both methods, and $NiFe_2O_4$ is insulating in both cases. The gap from the top of the valence band to the bottom of the conduction band is 2.2 eV (1.1 eV) within HSE06 (LSDA + U). The LSDA + U gap value is in good agreement with Refs. 19, 20, and 22. Further, the majority and minority channels are spin split in both the valence and conduction bands, as expected for a magnetic insulator, and we predict that the gap is larger in the majority channel than in the minority. The band gap from HSE06 (LSDA + U) is close to 3.3 eV (1.9 eV) for the majority band and 2.7 eV (1.6 eV) for the minority band, giving a 0.5 eV (0.3 eV) difference in the majority and minority band gaps. These findings are summarized in Table I. As expected, the exact numerical values depend on the screening length (in HSE) and U_{eff} (in LSDA + U) chosen in the calculation. For instance, increasing U_{eff} on the Ni and Fe sites diminishes and eventually eliminates the indirect gap in the minority channel of LSDA + U density of states, as the O p states remain fixed with respect to the Ni and Fe d states. Increasing or decreasing the screening length rigidly shifts the conduction bands without altering the qualitative structure. Both methods also predict that in the lowest-energy configuration, the octahedral sites (Ni and Fe) are aligned antiferromagnetically with the tetrahedral sites (Fe only), yielding fully compensated Fe moments with the net moment arising from the Ni centers.[21,22] The net unit cell moment is 2.0 μ_B per formula unit and is

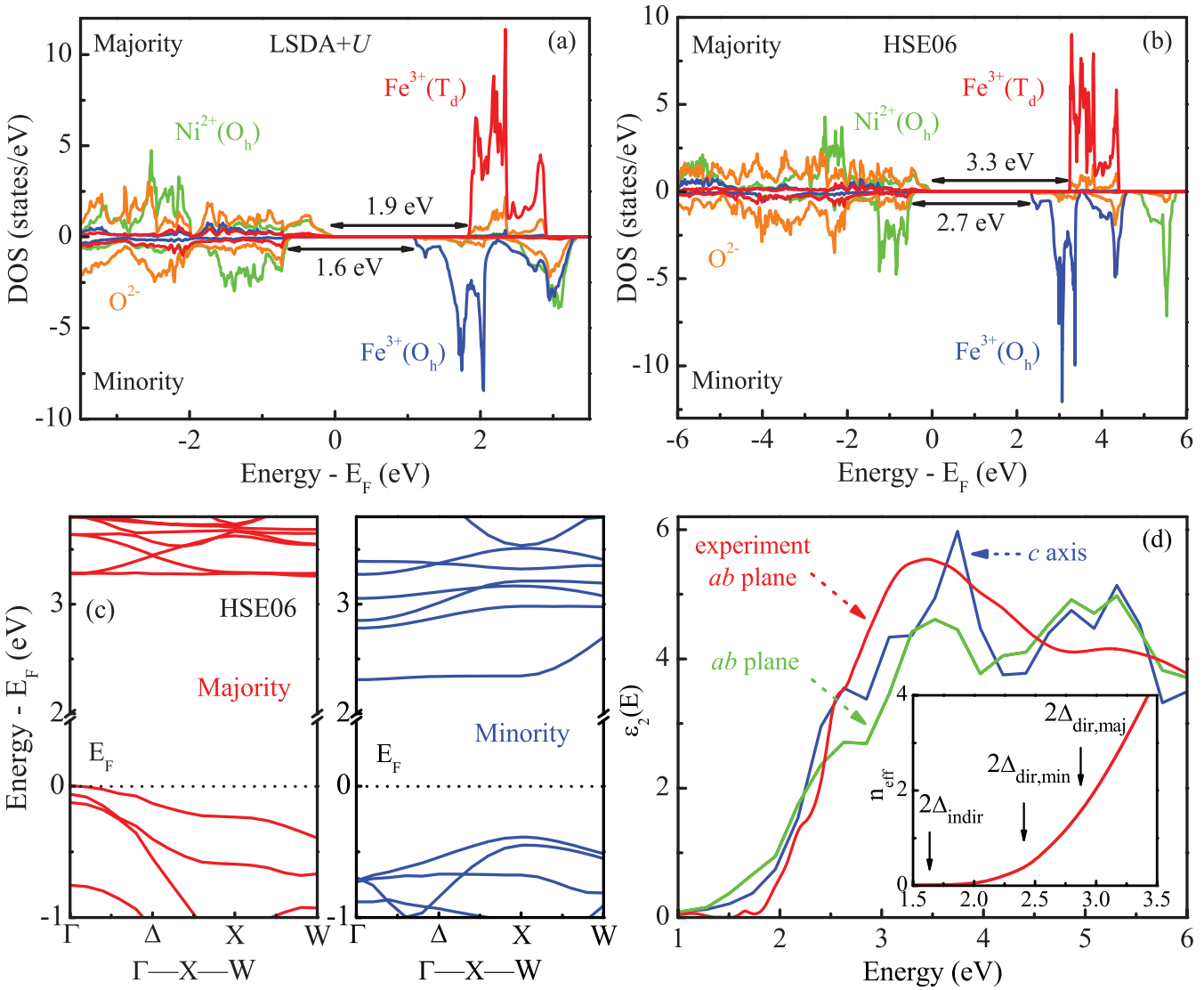

FIG. 1. (Color online) Density of states of $NiFe_2O_4$ calculated according to (a) the LSDA + U and (b) the screened hybrid functional HSE06 methods. The enhanced gap in the latter method is clearly seen. (c) HSE06 energy bands along Γ-X-W for majority (left) and minority (right) channels. The minority channel exhibits an indirect gap between X and Γ. In both channels, the lowest conduction band is nearly flat over a wide region, possibly leading to many nearly degenerate transitions (both direct and indirect). (d) Dielectric constant $\varepsilon_2(E)$ as a function of energy. Red curve: experimental spectrum; green curve: theoretical result in the *ab* plane; blue curve: theoretical result in the *c* direction. The agreement between calculated and experimental responses is reasonable. The inset shows the effective number of electrons n_{eff} as a function of energy. The various gaps are indicated.

TABLE I. Theoretical and measured optical band gap values of $NiFe_2O_4$ (in eV). These gaps overlap well with the solar spectrum.

	Band gap	HSE06	LSDA + U	Experimental gaps	
Indirect	$2\Delta_{\min}(X \rightarrow \Gamma)$	2.7	1.6	1.6	[from $(\alpha E)^{0.5}$ vs E plot]
Direct	$2\Delta_{\min}(X \rightarrow X)$	2.7	1.6	2.4	[from $(\alpha E)^2$ vs E plot]
	$2\Delta_{\min}(\Gamma \rightarrow \Gamma)$	3.0	1.6		
	$2\Delta_{maj}(\Gamma \rightarrow \Gamma)$	3.3	1.9	2.8	[from $(\alpha E)^2$ vs E plot]

consistent with this magnetic structure and the nominal valence states of Ni^{2+} and Fe^{3+}.

The LSDA + U and HSE partial density of states (DOS) [Figs. 1(a) and 1(b)] indicates that the narrow conduction band states belong to majority Fe d states and minority Fe and Ni d states. Despite the complexity of the material, the valence band can be neatly partitioned into deep and strongly localized Fe states (8 eV below Fermi level, not shown here) and predominantly Ni and O states near the Fermi level. In close analogy with the case of NiO,[38,39] hybridization smears the Ni and O states across the valence band, resulting in the highest occupied bands having both Ni d and O p characters. The minority Ni and O states, however, are more separated, and particularly in HSE06, the top of the valence band is dominated by a sharp Ni d peak, which is also found in NiO. The Fe states return to play a larger role in the conduction band, defining the size of the gap in both spin channels and thus reducing the gap compared with the NiO parent compound.

The charge transfer ($U > \Delta > W$) and Mott regimes ($\Delta > U > W$) are well-known limits of the Zaanen-Sawatzky-Allen classification scheme for insulating oxides.[40] Here, U is the on-site Coulomb repulsion, Δ is the ligand to metal charge transfer energy, and W is the bandwidth. Analysis of the states near the band edge reveals that $NiFe_2O_4$ displays both charge transfer (p-d) and Mott-Hubbard (intersite d-d) characters. In other words, it does not fall neatly into either limiting regime, a finding that makes this spinel interesting from the electronic structure point of view. Following the arguments of Ref. 40, this suggests that the Ni on-site d-d interaction U is roughly equal to the difference between the unoccupied Ni minority e_g and occupied O p energy levels. In $NiFe_2O_4$ or any similar material, the relevant quantities for determination of the charge-transfer gap are the unoccupied Fe d energy levels (both minority and majority) and occupied O p levels, while the correlation-induced gap depends on the magnitude of Fe on-site d-d and off-site O-Fe p-d, Fe-Fe d-d, and Ni-Fe d-d interactions.

To further investigate the nature of gaps, we plot the HSE06 bands [Fig. 1(c)] along the lines Γ-X-W for the majority (red, left) and minority (blue, right) channels. Both LSDA + U and HSE06 show a nearly flat conduction band in the majority channel exhibiting a direct gap at Γ (3.27 eV for HSE06, 1.90 eV for LDA + U). All indirect gaps in the majority channel lie higher in energy. The picture in the minority band is more complicated, with both indirect and direct gaps lying very close in energy. There is at least one indirect-gap candidate in the minority channel as the conduction band minimum lies at Γ while the valence band maximum is at the X point ($k = \frac{2\pi}{a}[100]$), the difference in energy being 2.70 eV (1.60 eV) in HSE06 (LSDA + U). Notable direct gaps just above the indirect gap are at X (2.73 eV for HSE06) and Γ (3.01 eV; Table I).

Figure 2 displays the 300 K optical absorption of two $NiFe_2O_4$ thin films prepared at different growth temperatures. There are only modest differences, so we focus our analysis on the highest-quality film grown at 690 °C. $NiFe_2O_4$ has a number of important dipole-allowed excitations in the optical response. Based on a comparison with the aforementioned electronic structure calculations, we can analyze the features in the optical data in terms of p-d and metal-to-metal intersite d-d charge-transfer-like excitations. We assign the strong band above 3 eV to a combination of majority channel d-d $Ni^{2+} \rightarrow Fe^{3+}(T_d)$ and p-d $O^{2-} \rightarrow Fe^{3+}(T_d)$ features. The edge of this band determines the majority channel direct gap, as discussed below. We attribute the 2.6 eV peak to the Γ-centered minority channel $O^{2-} \rightarrow Fe^{3+}(O_h)$ and $Ni^{2+} \rightarrow Fe^{3+}(O_h)$ charge transfer below the valence band maximum. The edge of this band [composed of $O^{2-} \rightarrow Fe^{3+}(O_h)$] determines the minority channel direct gap. Likewise, the absorption tail below 2.3 eV determines the minority channel indirect band gap, as discussed below. It is also a combination of p-d and d-d charge transfer processes. We assign the weak spectral features near

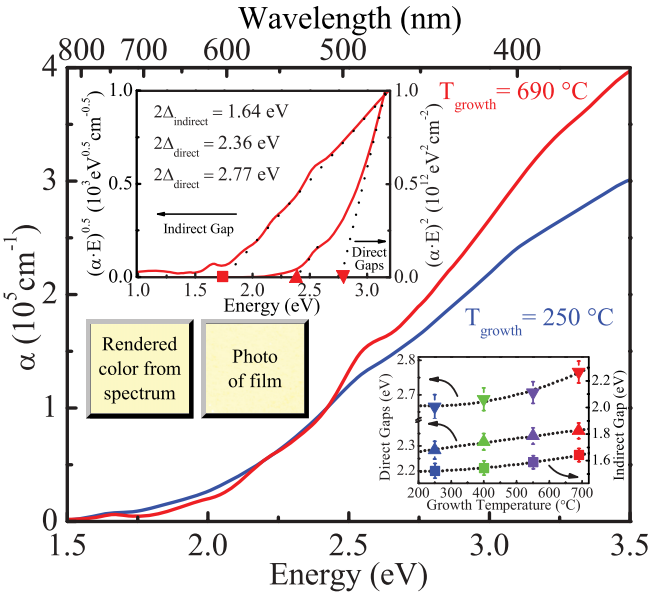

FIG. 2. (Color online) The 300 K absorption spectrum of $NiFe_2O_4$. The top left inset shows the optical band gap analysis for the film grown at 690 °C. The bottom left inset shows the rendered color[36] for the film grown at 690 °C compared to a photograph of the same film. The right inset shows the dependence of the direct and indirect optical band gaps on growth temperature.

2.2, 1.9, and 1.7 eV as on-site excitations of the metal centers.[41,42] It is these excitations along with the indirect edge, the 2.6 eV excitation, and the strongly rising edge near 3 eV that determine the color properties of this material. As shown in the bottom left inset of Fig. 2, the rendered color (calculated from the measured spectrum)[36] is in excellent agreement with a photo of the same film.

The theory of band gap analysis is well established for traditional semiconductors[37] and is commonly extended to oxides although under less rigorous conditions.[43,44] The top left inset of Fig. 2 summarizes our tests for indirect and direct band gap character in $NiFe_2O_4$. Importantly, we find evidence for both indirect and direct gaps in this material. Moreover, there is more than one direct gap. The consequences of these findings are discussed below.

$NiFe_2O_4$ is an indirect band gap system. A plot of $(\alpha E)^{0.5}$ vs energy (top left inset, Fig. 2) places the 300 K indirect optical band gap in our film at 1.64 ± 0.08 eV. We extract a coupling phonon energy[37] of $\sim$50 meV (400 cm^{-1}), which corresponds to the infrared active O-Fe-O bending mode.[23] This $(\alpha E)^{0.5}$ vs energy curve is fairly linear and displays a more characteristic shape than that of the 16 nm mesoporous sample measured by Haetge *et al.*,[26] likely because the tubular character of the sample disrupts the phonons and disallows this indirect gap. In other words, the 16 nm pores break the periodicity required to give the phonon coherent character, and a coupling phonon is required to have an indirect gap. Theoretically, the best candidate for this indirect gap is in the minority channel (from the valence band X point to the conduction band Γ point; Table I).

$NiFe_2O_4$ also has direct gaps. A plot of $(\alpha E)^2$ vs energy (top left inset, Fig. 2) places the 300 K direct optical band gaps in our film at 2.36 ± 0.05 and 2.77 ± 0.05 eV, which we assign to both minority and majority channel features based upon our first-principles results (see Table I). The direct band gaps are also similar to the values of 2.2 eV on a sintered bulk sample reported by Balaji *et al.*,[24] 2.5 eV on nanoparticles indicated by Dolia *et al.*,[25] and 2.7 eV on a 16 nm mesoporous sample reported by Haetge *et al.*[26] The values reported in Refs. 23 and 27 are outliers, probably due to sample quality issues.

Importantly, our analysis reveals that $NiFe_2O_4$ displays both indirect and direct band gaps. This is similar to the situation in Si and GaAs, which are well-known components of microelectronic devices.[23,37] The charge gap hierarchy and the overlap of these features with the solar spectrum suggest an additional application. Specifically, the difference between $2\Delta_{indir}$ and $2\Delta_{dir,maj}$ could provide an opportunity to obtain spin-polarized carriers via the excitation in the 1.64–2.77 eV energy range.[3,4] Such carriers could be photogenerated or injected and would presumably reside in the minority channel.

To quantify the strength of the various charge transfer excitations, we calculated the effective number of electrons involved in each transition, n_{eff}, using the partial sum rule: $n_{eff} = \int_{E_1}^{E_2} E\varepsilon_2(E)/(4\pi^2\hbar^2\epsilon_0)dE/(2\pi^2\omega_p^2)$, where $\varepsilon_2(E)$ is the dielectric constant data of Fig. 1(d), $\omega_p = \sqrt{e^2/V_0 m\epsilon_0}$ is the plasma frequency, e and m are the charge and mass of an electron, ϵ_0 is the vacuum dielectric constant, V_0 is the unit-cell volume, and E_1 and E_2 are the limits of integration.[35] As shown in the inset of Fig. 1(d), n_{eff} is small below the indirect band gap because there are no electric dipole allowed transitions in this range. Above $2\Delta_{indir} = 1.64$ eV, n_{eff} increases gradually, a process that depends on phonon coupling, as discussed above. The effective number of electrons increases more rapidly above $2\Delta_{dir,min} = 2.36$ eV, and the slope of n_{eff} is even larger above $2\Delta_{dir,maj} = 2.77$ eV as the absorbed photons activate various charge transfer processes. Photoconductivity experiments could test this proposal.

The main effect of decreasing growth temperature is that the features are smeared out and the spectrum is more diffuse. The right inset of Fig. 2 summarizes the growth temperature dependence of the indirect and direct band gaps of $NiFe_2O_4$. The gradual red shifts with decreasing film growth temperature are consistent with a simple structural decoherence picture.[18,33] The trends also correlate with the finding that the low-temperature film is more strained than the high-temperature film,[18,20] although there is no dramatic strain dependence. The limited effect of growth temperature on the various gaps suggests that if main goal is to maintain the gap values, one can sacrifice structural fidelity for easier processing.

IV. CONCLUSIONS

To summarize, we combined first-principles calculations, optical spectroscopy, and film growth studies to comprehensively investigate the electronic band gap of $NiFe_2O_4$. This spinel oxide is an indirect band gap material which theory assigns to the minority spin channel, with two higher-lying direct gaps in the minority and majority channels, respectively. This series of gaps emanates from the flatness of the bands. Analysis of the states near the band edge reveals a combination of p-d and d-d charge transfer characters in both channels, with transitions into and between the correlated bands of the Ni^{2+} and Fe^{3+} sites. This leads to a system that is not easily classified within the Zaanen-Sawatsky-Allen scheme.

ACKNOWLEDGMENTS

This research is supported by the US Department of Energy, Office of Basic Energy Sciences, Division of Materials Sciences and Engineering under Award No. DE-FG02-01ER45885 (J.L.M.). Work at the University of Alabama is supported by a NSF-NRI supplement as part of NSF MRSEC Grant No. DMR-0213985 (A.G., W.H.B.). We thank J. Cao for useful discussions.

*gkim@mint.ua.edu

[1] G. F. Dionne, *Magnetic Oxides* (Springer, New York, 2009).

[2] Y. Kajiwara, K. Harii, S. Takahashi, J. Ohe, K. Uchida, M. Mizuguchi, H. Umezawa, H. Kawai, K. Ando, K. Takanashi, S. Maekawa, and E. Saitoh, Nature (London) **464**, 262 (2010).

[3] I. Zutic, J. Fabian, and S. Das Sarma, Rev. Mod. Phys. **76**, 323 (2004).

[4] S. A. Wolf, D. D. Awschalom, R. A. Buhrman, J. M. Daughton, S. von Molnar, M. L. Roukes, A. Y. Chtchelkanova, and D. M. Treger, Science **294**, 1488 (2001).

[5]D. C. Worledge and T. H. Geballe, J. Appl. Phys. **88**, 5277 (2000).
[6]J. S. Moodera, G.-X. Miao, and T. S. Santos, Phys. Today **63**(4), 46 (2010).
[7]J. C. Slonczewski, Phys. Rev. B **82**, 054403 (2010).
[8]G. F. Dionne, J. Appl. Phys. **63**, 3777 (1988).
[9]The unit cell is cubic [$a = 8.3379(3)$ Å at 300 K] with 8 formula units and a $Fd\bar{3}m$ space group. It displays a fully inverted spinel structure with the general formula AB_2O_4 where A and B denote tetrahedral (T_d) and octahedral (O_h) cation sites in a close-packed oxygen environment.
[10]D. Fritsch and C. Ederer, Appl. Phys. Lett. **99**, 081916 (2011).
[11]V. I. Anisimov, F. Aryasetiawan, and A. I. Lichtenstein, J. Phys. Condens. Matter **9**, 767 (1997).
[12]A. Svane and O. Gunnarsson, Phys. Rev. Lett. **65**, 1148 (1990).
[13]J. Heyd, G. E. Scuseria, and M. Ernzerhof, J. Chem. Phys. **118**, 8207 (2003).
[14]J. Heyd, J. E. Peralta, G. E. Scuseria, and R. L. Martin, J. Chem. Phys. **123**, 174101 (2005).
[15]F. Tran and P. Blaha, Phys. Rev. Lett. **102**, 226401 (2009).
[16]M. Shishkin, M. Marsman, and G. Kresse, Phys. Rev. Lett. **99**, 246403 (2007).
[17]A. Walsh, S. H. Wei, Y. Yan, M. M. Al-Jassim, J. A. Turner, M. Woodhouse, and B. A. Parkinson, Phys. Rev. B **76**, 165119 (2007).
[18]M. N. Iliev, D. Mazumdar, J. X. Ma, A. Gupta, F. Rigato, and J. Fontcuberta, Phys. Rev. B **83**, 014108 (2011).
[19]V. N. Antonov, B. N. Harmon, and A. N. Yaresko, Phys. Rev. B **67**, 024417 (2003).
[20]D. Fritsch and C. Ederer, Phys. Rev. B **82**, 104117 (2010).
[21]J. M. Hastings and L. M. Corliss, Rev. Mod. Phys. **25**, 114 (1953).
[22]Z. Szotek, W. M. Temmerman, D. Ködderitzsch, A. Svane, L. Petit, and H. Winter, Phys. Rev. B **74**, 174431 (2006).
[23]R. D. Waldron, Phys. Rev. **99**, 1727 (1955).
[24]S. Balaji, R. K. Selvan, L. J. Berchmans, S. Angappan, K. Subramanian, and C. O. Augustin, Mater. Sci. Eng. B **119**, 119 (2005).
[25]S. N. Dolia, R. Sharma, M. P. Sharma, and N. S. Saxena, Indian J. Pure Appl. Phys. **44**, 774 (2006).
[26]J. Haetge, C. Suchomski, and T. Brezesinski, Inorg. Chem. **49**, 11619 (2010).
[27]R. C. Rai, S. Wilser, M. Guminiak, B. Cai, and M. L. Nakarmi, Appl. Phys. A **106**, 207 (2012).
[28]G. Kresse and J. Furthmüller, Comput. Mater. Sci. **6**, 15 (1996).
[29]G. Kresse and D. Joubert, Phys. Rev. B **59**, 1758 (1999).
[30]J. Paier, M. Marsman, K. Hummer, G. Kresse, I. C. Gerber, and J. G. Angyan, J. Chem. Phys. **124**, 154709 (2006).
[31]Z. Zhang and S. Satpathy, Phys. Rev. B **44**, 13319 (1991).
[32]P. E. Blöchl, Phys. Rev. B **50**, 17953 (1994).
[33]J. X. Ma, D. Mazumdar, G. Kim, H. Sato, N. Z. Bao, and A. Gupta, J. Appl. Phys. **108**, 063917 (2010).
[34]R. E. Glover and M. Tinkham, Phys. Rev. **108**, 243 (1957).
[35]F. Wooten, *Optical Properties of Solids* (Academic, New York, 1972).
[36]R. S. Berns, *Principles of Color Technology*, 3rd ed. (Wiley, New York, 2000).
[37]J. I. Pankove, *Optical Processes in Semiconductors* (Dover, New York, 1971).
[38]F. Aryasetiawan and O. Gunnarsson, Phys. Rev. Lett. **74**, 3221 (1995).
[39]T. M. Schuler, D. L. Ederer, S. Itza-Ortiz, G. T. Woods, T. A. Callcott, and J. C. Woicik, Phys. Rev. B **71**, 115113 (2005).
[40]J. Zaanen, G. A. Sawatzky, and J. W. Allen, Phys. Rev. Lett. **55**, 418 (1985).
[41]B. I. G. F. Henderson, *Optical Spectroscopy of Inorganic Solids* (Oxford University Press, New York, 1989).
[42]L. L. Lohr, Coord. Chem. Rev. **8**, 241 (1972).
[43]K. H. Kim, K. C. Park, and D. Y. Ma, J. Appl. Phys. **81**, 7764 (1997).
[44]X. S. Xu, J. F. Ihlefeld, J. H. Lee, O. K. Ezekoye, E. Vlahos, R. Ramesh, V. Gopalan, X. Q. Pan, D. G. Schlom, and J. L. Musfeldt, Appl. Phys. Lett. **96**, 192901 (2010).